Intermodulation Distortion in Pseudomorphic HEMT's and an Extension of the Classical Theory

Michael Jon Bailey, *Member, IEEE*

***Abstract*—Pseudomorphic high electron-mobility transistors (pHEMT's) offer superior RF and microwave performance and, in particular, exhibit exceptional intermodulation distortion characteristics that are not adequately modeled by the classical theory. Intermodulation products are typically 8–10 dB below classical expectations, and can be as much as 12 dB lower. An extension of the classical theory is presented, which allows for a better understanding of this phenomenon in terms of the device transconductance characteristic. Experimental data is included to provide quantitative verification based on both device and amplifier results. pHEMT-based devices have the potential to satisfy the spectral performance requirements of today's wireless systems with improved dc-to-RF efficiencies.**

***Index Terms*—HEMT, intermodulation distortion, semiconductor devices.**

I. Introduction

THE requirements of modern digital wireless communications systems place stringent demands on the inherent linearity of active devices, and this trend can be expected to continue as systems evolve to support the increasing subscriber base. Systems designed to accommodate multiple simultaneous users over a widespread area must maximize spectral efficiency. Power amplifiers for handsets, for example, need to satisfy conflicting requirements of dc-to-RF efficiency, output power, and minimal spectral regrowth. The IS-95 and IS-98 CDMA reverse-link standard requires a +28-dBm output power (offset QPSK modulation) with adjacent channel power at least −42 dBc at ±885-kHz offset, with a 1.23-MHz channel bandwidth [1]. For the forward link (base station to handset), the requirement is more severe since the modulation is QPSK with a 10-dB peak-to-average power envelope. The reverse-link handset condition only requires a 3-dB peak-to-average envelope since the base station must accommodate a multicarrier transmission mode, whereas the handset does not. Since spectral regrowth is a direct result of amplifier nonlinearities with continuous spectra input signals (i.e., pseudorandom modulation), the standard approach is to operate the power amplifier considerably below its rated output power level, usually defined as the output power at 1 dB of gain compression ($P_{1\,\mathrm{dB}}$). This use of output backoff to ensure tolerable spectral regrowth results in poor dc-to-RF efficiency, thereby limiting transmit time for battery-powered handset units.

Manuscript received January 27, 1999.
The author is with Filtronic Solid State, Santa Clara, CA 95054-3095 USA.
Publisher Item Identifier S 0018-9480(00)00222-2.

The classical and still widely used benchmark for device and system linearity is based on memoryless linear network theory. In this first-order theory, a small amount of nonlinearity is added, creating a "near-linear" network, and this network's intermodulation distortion (IMD) behavior is related to its power transfer curve. This theory adequately models the AM-to-AM conversion characteristics of most active devices, and establishes the useful concept of the third-order intercept point (IP3). Nonlinear reactance effects also inherent in most active devices generate AM-to-PM effects, but it has been demonstrated that AM-to-AM effects dominate the spectral regrowth near the carrier, i.e., within the adjacent channels [2]. It remains unclear whether or not standard IMD measurements can be quantitatively related to spectral regrowth, and so direct measurements of adjacent channel power ratio (ACPR) are required. Nonetheless, the theory of IMD and IP3 concept provides for a simple and powerful description of device linearity.

The classical theory adequately describes the characteristics of a wide range of active devices and, thus, the IP3 measurement is standard for devices including the GaAs MESFET, the Si MOSFET (and variants), the bipolar junction transistor (BJT), or the newer heterojunction bipolar transistor (HBT). However, as will be demonstrated in this paper, the classical linearity theory is inadequate to describe the behavior of certain types of devices, as exemplified by the pseudomorphic high electron-mobility transistor (pHEMT). An extended theory is now presented, in which it is demonstrated that some classes of devices, and the pHEMT in particular, offer significantly improved linearity performance over a wide dynamic range.

II. The Classical Theory

The classical theory of linear and near-linear systems has been described in a number of sources (as found, for example, in [3]), and it is useful to review the salient features of this theory. A linear or distortion-free two-port memoryless system will accept an input signal and produce an output signal that is a scaled version of the input, differing only in amplitude and possibly a constant phase shift. This means that the system transfer function $H(j\omega)$ is given by

$$H(j\omega) = K \exp(-j\omega t_o) \tag{1}$$

where K and t_o are constants. Real amplifiers may be classed as near-linear two-port systems, i.e., with a small amount of

nonlinearity. In this case, the two-port's voltage gain may be approximated by the expansion

$$e_o = k_1 e_i + k_2 e_i^2 + k_3 e_i^3 + \cdots \tag{2}$$

where e_i is the input signal, e_o is the output signal, and $k_{1,2,3}$ is the expansion series coefficients. A single sinusoidal input signal of the form is assumed as follows:

$$e_i = A \cos \omega_1 t \tag{2a}$$

where A is the input signal amplitude (volts), ω_1 is $2\pi f_1$, and f_1 is the signal frequency. Expanding this series and combining like terms, the resulting output signal consists of a dc component, and components at the fundamental, second, and third harmonic frequency (ω_1, $2\omega_1$, and $3\omega_1$). The fundamental component at ω_1 has an amplitude which is, in dBm units, as follows:

$$P_o = 10 \log \left\{ \left(\frac{k_1 A + \frac{3}{4} k_3 A^3}{\sqrt{2}} \right)^2 \frac{10^3}{R} \right\} \tag{3}$$

where $R =$ load impedance (ohms). The resulting power gain for the two-port becomes

$$G = 20 \log \left(k_1 + \frac{3}{4} k_3 A^2 \right) \tag{4}$$

where $G =$ power gain, compared to the linear power gain: $G_o = 20 \log k_1$. The power-gain expression (4) allows for gain expansion ($k_3 > 0$), or gain compression ($k_3 < 0$), but not both. Practical amplifiers are typically characterized by their output power at the point of 1-dB gain compression, compared to the linear gain; and this is given by (dBm units)

$$P_{1\,\mathrm{dB}} = 10 \log \left\{ \frac{k_1^3}{|k_3|} \right\} + 0.62. \tag{5}$$

III. IMD

The near-linear two-port generates harmonics, but the lowest harmonic at $2\omega_1$ is generally outside the system bandwidth in most cases; however, if multiple input signals are present, IMD products will be generated within the typical system bandwidth. The standard method for characterizing this type of nonlinearity is the two-tone IMD test. Two carriers of equal amplitude, at f_1 and f_2, are applied to the two-port under test, and the third-order intermodulation products at $2f_1 - f_2$ and $2f_2 - f_1$ are measured relative to the fundamental tones. Substitution of the two-tone input signal

$$e_i = A \cos \omega_1 t + A \cos \omega_2 t \tag{6}$$

into (2) yields an expression that contains the third-order IMD terms

$$e_0 = \frac{3}{4} k_3 A^3 \cos (2\omega_1 - \omega_2) t + \frac{3}{4} k_3 A^3 \cos (2\omega_2 - \omega_1) t + \cdots \tag{7}$$

and, therefore, the power levels of the third-order IMD products are, in dBm units, as follows:

$$P_{3\mathrm{rd}} = 10 \log \left\{ \left(\frac{3 k_3 A^3}{4\sqrt{2}} \right)^2 \frac{10^3}{R} \right\}. \tag{8}$$

Note that the third-order IMD products increase with a slope of 3:1 with respect to the fundamental tone output power by comparison with the $k_1 A$ term of (3). The linear extrapolation of (3) intersects with the IMD power expression (8) at a point that is defined as the IP3, given by (dBm units)

$$P_{IP} = 10 \log \left(\frac{2 k_1^3}{3 k_3} \cdot \frac{10^3}{R} \right). \tag{9}$$

The IP3 can be related to the P_{1dB} power level by combining equations (9) and (5), resulting in

$$P_{IP} = P_{1\,\mathrm{dB}} + 10.63\ \mathrm{dB}. \tag{10}$$

This well-known result, which specifies that a near-linear two-port's intercept point is approximately 10 dB above the 1-dB compression power level, is extremely useful since it only requires a single-tone power characterization of the device-under-test. In the presence of two carriers, the power-gain expression (4) is modified, as the numeric coefficient of the k_3 term becomes $9/4$. Note that (9) stipulates that the IP3 is a constant, and by combining this expression with (8) yields the two other well-known relationships as follows:

$$P_{3\mathrm{rd}} = 3P_{\omega_1} - 2P_{IP} \tag{11a}$$

and

$$P_{IP} = \frac{1}{2} (3P_{\omega_1} - P_{3\mathrm{rd}}). \tag{11b}$$

IV. The Extended Theory

The classical theory is now extended by including two additional higher order terms in (2) as follows:

$$e_o = k_1 e_i + k_2 e_i^2 + k_3 e_i^3 + k_4 e_i^4 + k_5 e_i^5 + \cdots. \tag{12}$$

For a single-tone input of the form (2a), this gives

$$\begin{aligned} e_0 = {} & \frac{1}{2} k_2 A^2 + \frac{3}{8} k_4 A^4 + \left\{ k_1 A + \frac{3}{4} k_3 A^3 + \frac{5}{8} k_5 A^5 \right\} \\ & \cdot \cos (\omega t) + \left\{ \frac{1}{2} k_2 A^2 + \frac{1}{2} k_4 A^4 \right\} \\ & \cdot \cos (2\omega t) + \left\{ \frac{1}{4} k_3 A^3 + \frac{5}{16} k_5 A^5 \right\} \\ & \cdot \cos (3\omega t) + \frac{1}{8} k_4 A^4 \cos (4\omega t) \\ & + \frac{1}{16} k_5 A^5 \cos (5\omega t) + \cdots. \end{aligned} \tag{13}$$

This leads to a new expression for the fundamental power gain

$$G_P^{\mathrm{ext}} = 20 \log \left(\frac{e_o}{e_i} \right) = 20 \log \left\{ k_1 + \frac{3}{4} k_3 A^2 + \frac{5}{8} k_5 A^4 \right\}. \tag{14}$$

Note that this new expression allows for gain expansion followed by compression, with $k_3 > 0$ and $k_5 < 0$. Devices that exhibit little or no gain expansion are adequately modeled by (4). The location of the peak gain expansion can be determined by converting (14) to a voltage gain expression, and setting the first derivative equal to zero, yielding

$$A_{PK} = \sqrt{\frac{3k_3}{5|k_5|}}. \tag{15}$$

For a two-tone input signal of the form (6), the extended power series (12) gives the following:

$$\begin{aligned} e_0 = &\left\{k_1 + \frac{9}{4}k_3A^3 + \frac{25}{4}k_5A^5\right\}\cos(\omega_1 t) \\ &+ \left\{k_1 + \frac{9}{4}k_3A^3 + \frac{25}{4}k_5A^5\right\}\cos(\omega_2 t) \\ &+ \left\{\frac{3}{4}k_3A^3 + \frac{25}{8}k_5A^5\right\}\cos\left[(2\omega_1 - \omega_2)t\right] \\ &+ \left\{\frac{3}{4}k_3A^3 + \frac{25}{8}k_5A^5\right\}\cos\left[(2\omega_2 - \omega_1)t\right] + \cdots. \end{aligned} \tag{16}$$

This expression is derived in more detail in the Appendix. Inspection of (16) shows that the two-tone fundamental power gain is not equal to the single-tone gain, by comparison of the k_3 and k_5 terms; this is true even in the case of no gain expansion, i.e., the standard theory. This is not a new result, having been derived in general terms by Blachman [4]. The terms for the third-order IMD products now contain an explicit relationship to the k_5 coefficient, and since $k_5 < 0$ (for devices with gain expansion), there exists the possibility of significant reduction in the power level of the IMD products.

The suppression of IMD levels by higher order expansion coefficients has been explored before, e.g., in GaAs MESFET's with specially tailored doping profiles, as described in [5]. To analyze these engineered devices, the authors began with power series expansions of the transconductance, input capacitance, and drain conductance, which were then utilized to predict the ratio of third-order IMD products to the fundamental signal levels. The resulting IP3 improvement shown by these devices was on the order of 3–4 dB, at least for low-input signal levels; by contrast, pHEMT's have demonstrated 10–12 dB of IP3 enhancement over a much wider range of input power levels. In this paper, the single-tone AM-to-AM characteristics of a generalized device, specifically the presence of gain expansion, is related to the two-tone IMD behavior.

The extended theory's salient features are summarized in Fig. 1. Over a wide range of input power levels, the third-order intermodulation products are suppressed in comparison to the classical theory. The classical behavior holds that the IP3 is constant when the device is operated in its "linear" region, but in the extended theory, the IP3 is not strictly constant and, consequently, the concept of IP3 may no longer be as useful. Examination of (16) shows that the IMD products are completely cancelled at an input signal amplitude given by

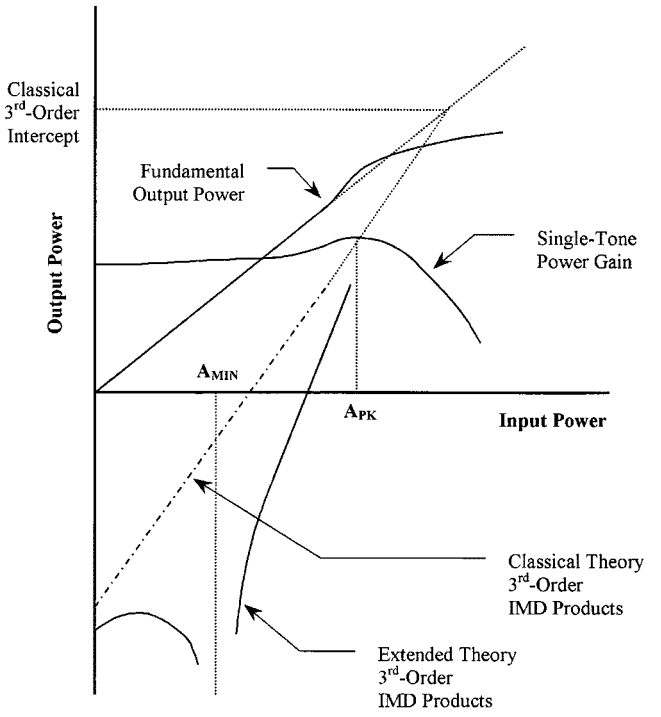

Fig. 1. Notional summary of the extended theory. IMD products are predicted to be considerably lower than classical expectations over a wide range of input power levels.

$$A_{\text{MIN}} = \frac{1}{5}\sqrt{\frac{3k_3}{|k_5|}}. \tag{17}$$

This input signal amplitude is about 5–7 dB below A_{PK} (15), the point of peak power gain expansion and, therefore, this represents the optimum backoff for minimizing the IMD products. At input signal amplitudes approximately 20–25 dB below A_{PK}, the k_3 component dominates the third-order terms, and the IMD products approach the classical result in (8).

V. Linear Operation and the Transconductance Characteristic

For the GaAs MESFET and other devices with similar transconductance characteristics, determining the quiescent operating point (OP) for optimum linear operation is fairly straightforward. By inspection of the equivalent-circuit model for a generic FET [6], the small-signal admittance matrix may be generated, which can be converted to the $ABCD$ representation [7]. Considering only the intrinsic device parameters, and assuming that a conjugate match exists on both the input and output of the device, the voltage gain may be expressed as

$$a = \frac{e_o}{e_i} = \frac{g_M R_L}{1 + g_{\text{DS}} R_L} \tag{18}$$

where g_M is the transconductance, g_{DS} is the output conductance, and R_L is the load resistance. In this simplified intrinsic expression, the transconductance characteristic determines the voltage gain, which is central to the foregoing discussion. Figs. 2 and 3 depict notional I–V and transconductance characteristics

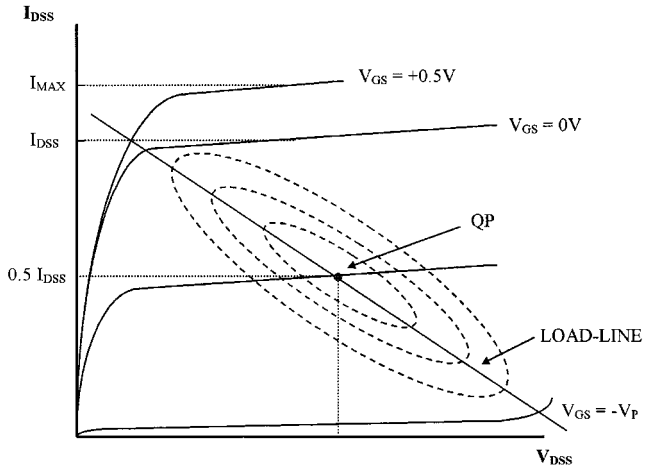

Fig. 2. Notional MESFET I–V curves ($I_{\rm DS}$ versus $V_{\rm DS}$). The external matching circuit provides the load line as shown; also shown are dynamic load lines at three levels of output power, centered on the quiescent OP.

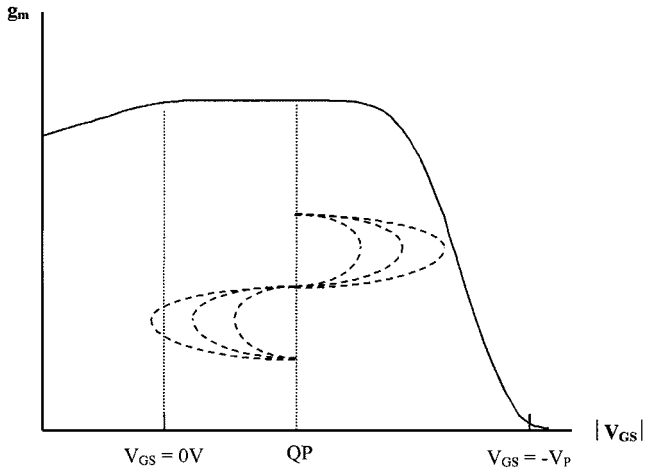

Fig. 3. Typical MESFET transconductance characteristic, plotted from a slightly positive gate bias to pinchoff. Three input signal levels are shown centered on the quiescent OP; a sufficiently large drive level causes a reduction in the average g_m, resulting in gain compression.

for a GaAs MESFET device. Since the MESFET is a depletion-mode device, the usual choice for Class-A operation is to operate at 50% of $I_{\rm DSS}$ (saturated drain–source current at $V_{\rm GS} = 0$ V), with a drain-to-source voltage centered between the "knee" voltage (the linear to saturation transition) and the gate–drain breakdown voltage. With a suitable choice of the load line, this quiescent OP allows for maximum voltage and current swing without clipping of the amplified signal. The maximum theoretical dc-to-RF efficiency for such a Class-A amplifier is 50% for a sinusoidal input signal. Fig. 2 shows the OP and dynamic load lines, representing the locus traced by an RF signal, for three different input power levels; it is clear that driving the device with a sufficiently large input signal will result in overdrive, with clipping of the voltage waveform. Practical MESFET amplifiers will, however, exhibit greater efficiencies when driven into saturation, although with significant signal distortion.

Shown in Fig. 3 is a typical transconductance (g_m) curve for the uniformly doped MESFET, as discussed in [8, pp. 334–334]. Note that there is a region of relatively constant g_m, and for small-to-moderate input signal levels, the MESFET will operate

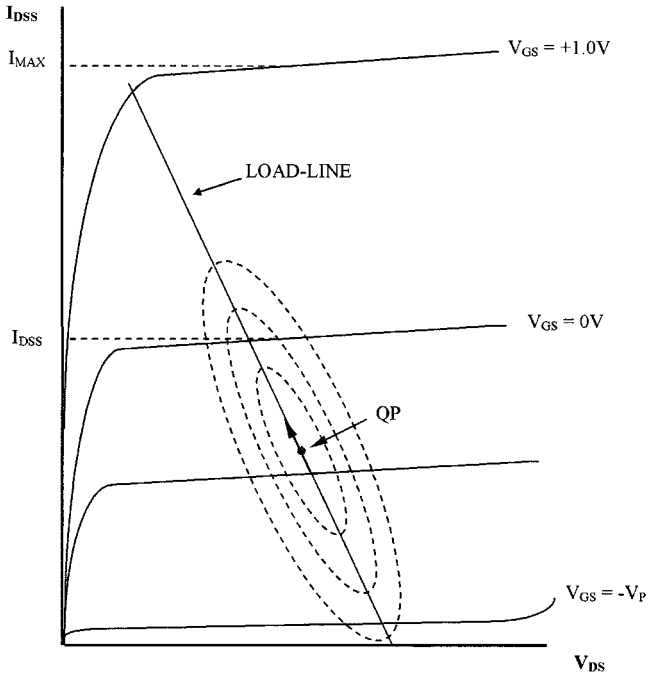

Fig. 4. Notional I–V curves for the pHEMT. Note the large value of $I_{\rm MAX}$ relative to $I_{\rm DSS}$; the ratio $I_{\rm MAX}/I_{\rm DSS}$ can be as high as 2 : 1. Asymmetry in the transconductance contour (see Fig. 5) about the OP result in current "drive up" as the input signal increases.

linearly, i.e., the power gain will be constant with drive level. As the input drive level increases, however, the average g_m during each RF cycle will begin to decrease, and the power gain begins to compress. Selection of a bias point less than 50% of $I_{\rm DSS}$ will allow for increased efficiency, but clipping of the amplified waveform, and generation of harmonics will result; this is precisely the case for Class-AB, Class-B, or Class-C operation. A quiescent bias point within the constant-g_m region will have one additional consequence, which is that the device will exhibit little or no current "drive-up" as drive level is increased since such an OP is symmetric with respect to current.

VI. The pHEMT and Related Devices

Figs. 4 and 5 present notional I–V and g_m curves for a typical pHEMT device [9].[1] There are a number of important differences compared to the MESFET and, in particular, the g_m characteristic does not have a region of constant g_m. The other striking aspect is the large amount of current when a positive bias is applied to the gate, a consequence of the charge–control mechanism intrinsic to the pHEMT. In the case of the MESFET, a small amount of positive gate bias reduces the depletion region, resulting in the maximum possible saturated current. The pHEMT does not share this limitation, and the devices generally will go into forward gate conduction before a maximum current limit is reached (although this depends on the specifics of the epitaxial structure). Operation at the standard Class-A bias point of 50% of $I_{\rm DSS}$ generally yields power-added efficiency exceeding 50%, and the pHEMT will also exhibit gain expansion and current drive up. In Fig. 4, the current denoted as $I_{\rm MAX}$ (defined as the saturated drain–source current with $V_{\rm GS} = +1.0$ V)

[1]Available HTTP: http://www.filtronicsolidstate.com

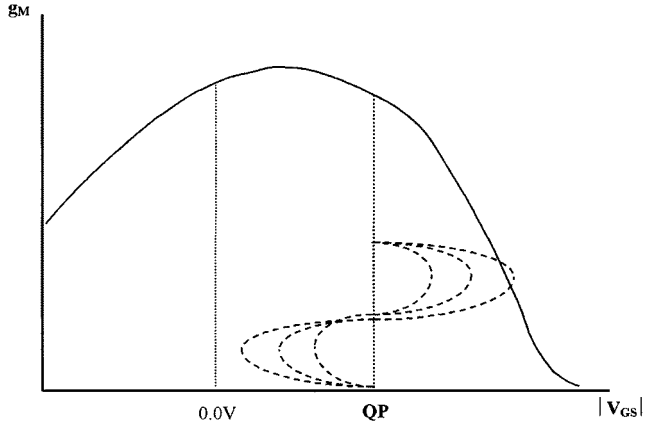

Fig. 5. pHEMT transconductance characteristic. The g_M is asymmetric with respect to the OP. The average g_M will increase with input signal level.

can be as much as 170%–220% of $I_{\rm DSS}$ and, therefore, the usual Class-A condition (50% of $I_{\rm DSS}$) is not symmetric with respect to the family of I–V curves. The point of current symmetry for the pHEMT is generally 75%–90% of $I_{\rm DSS}$.

The pHEMT's unique transconductance characteristic underlies the unusual IMD performance of these devices since it follows from the extended theory that, if the intrinsic voltage gain of a device possesses nonzero higher order derivatives, cancellation of the IMD products will be possible. There exists a wide range of bias conditions for the pHEMT that satisfy these conditions. In the case of the MESFET, biasing at or near pinchoff may result in some IMD product cancellation, but at larger input signal levels, the device will begin to clip the voltage waveform, with subsequent IMD degradation.

VII. Experimental Results

Qualitative confirmation of the extended theory's predictions have been noted in a wide variety of applications; in general, when a quiescent OP in the range of 20%–60% of $I_{\rm DSS}$ is used, IMD products are typically 5–12 dB below classical expectations. Reverting to the concept of IP3, reported IP3 values are consequently 15–22 dB higher than $P_{1\,\rm dB}$, compared to the classical "10-dB" rule. The quantitative results presented here were taken from an amplifier based on the LP1500 pHEMT device (manufactured by Filtronic Solid State, Santa Clara, CA), and can be considered fairly representative.

The LP1500 is a double-heterojunction discrete pHEMT with gate dimensions of 0.25 μm x 1500 μm, which is normally utilized as a high-performance power device, with a standard bias condition of $V_{\rm DS} = 8$ V, $I_{\rm DS} = 50\%\ I_{\rm DSS}$. In the low-noise high dynamic range application, the typical bias conditions used are $V_{\rm DS} = 5$ V, $I_{\rm DS} = 25\%\ I_{\rm DSS}$. The data presented in Figs. 6–8 were taken on a 1900-MHz amplifier based on this device, with simple single-pole input and output matching circuits and a shunt-series *R*–*L* stabilization network. At this bias condition, the LP1500 can be tuned to achieve a typical linear power of 22–24 dBm; however, no effort was made in this case to obtain a proper power match or to provide for harmonic tuning.

Fig. 6 presents the amplifier's measured power gain compared to the classical and extended theory relationships (4) and

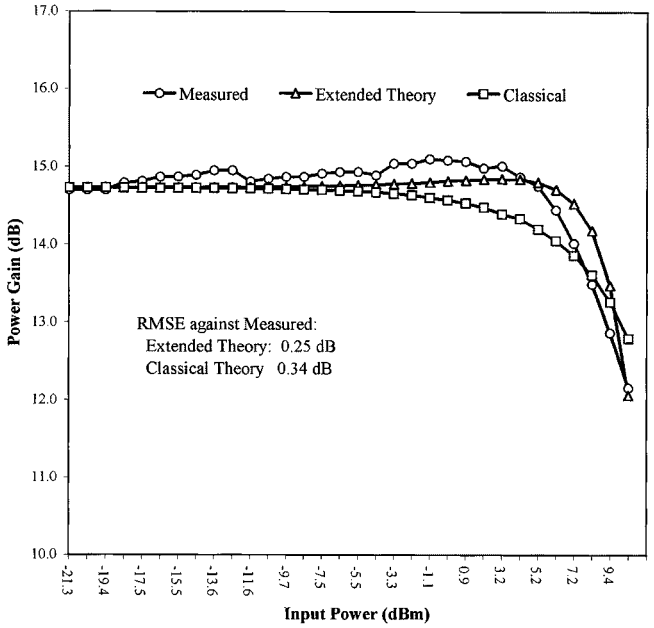

Fig. 6. Power gain data taken on the pHEMT-based 1900-MHz amplifier. Varying the expansion and compression coefficients, i.e., k_3 and k_5 from (14), the extended-theory power-gain expression is fitted to the measured data. The classical expression, (4) is set to match the actual power at 1 dB of gain compression. Root-mean-square error (rms) values for both models versus measured data are given.

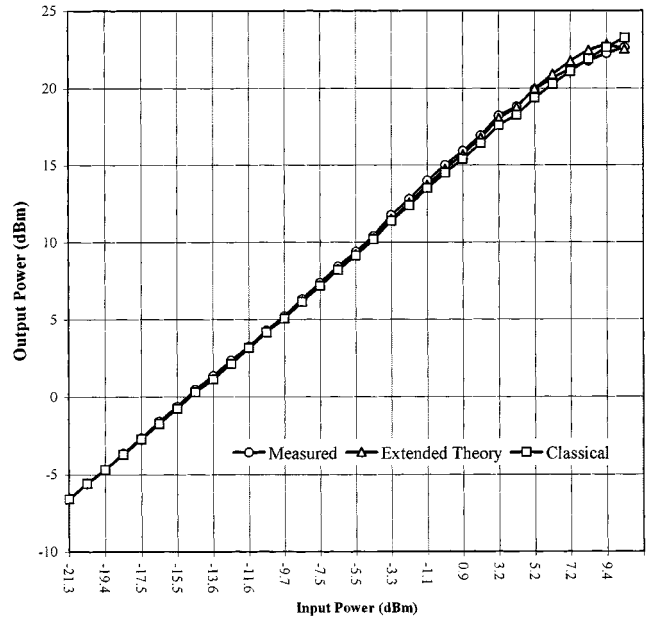

Fig. 7. Power transfer curves. The modeled curves use the actual input power levels. The measured $P_{1\,\rm dB} = 21.5$ dBm and, therefore, the expected classical $IP3 = 32.1$ dBm.

(14). In the case of the classical theory, k_1 and k_3 were adjusted to match the actual $P_{1\,\rm dB}$ and small-signal gain. Modeling the power gain with (14) was accomplished by successive iterations of k_3 and k_5, noting that the overall magnitude of the coefficients sets the predicted IMD product power levels (16), while the ratio of k_3 to k_5 fixes the peak of the gain expansion. Clearly, the classical power-gain expression does not account for the measured 0.4 dB of gain expansion, whereas the (16) provides a

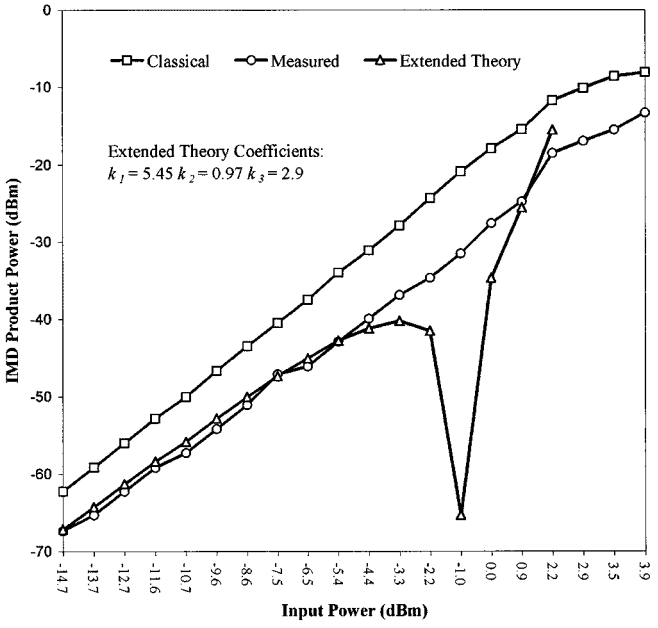

Fig. 8. Measured two-tone IMD data, the extended theory prediction, and the expected performance based on the classical theory and an assumed IP3 of 32.1 dBm. Actual pHEMT IMD performance is typically 8–10 dB lower than classical theory, even in the region of gain compression. The predictions of the extended theory begin to diverge as the device goes into gain compression.

fairly good model well into saturation (note the rms values calculated against the measured data). Fig. 7 presents the measured single-tone power transfer curve plotted against the predictions of the two models (using the actual input power levels).

The measured IMD performance of this example amplifier is plotted in Fig. 8, along with the predictions of (16), and the expected performance from the classical theory. The classical behavior given by (11a) is plotted based on the measured $P_{1\,\mathrm{dB}}$ of 21.5 dBm, and an assumed IP3 of 32.1 dBm. Once again, the classical theory cannot account for the measured IMD product power levels, which are 8–10 dB lower than expected; the amplifier behaves as if the IP3 was 40–42 dBm. The extended theory models the measured data reasonably well up to the onset of gain compression. The subject amplifier in this example did not show the complete cancellation of IMD products as predicted, but does show a small localized decrease. As the device begins to transition into large-signal operation, other factors that have not been modeled begin to become significant; this is discussed in more detail in Section VIII.

Another very significant finding is that the IMD behavior of the pHEMT remains far below classical expectations even as the device approaches gain compression and saturation. It is clear that there are additional cancellation mechanisms that need to be identified and analyzed. Table I presents a brief summary of measured or reported IMD performance results obtained on several discrete pHEMT devices at various frequencies in a number of applications.

Recent results on high-power multistage pHEMT-based amplifiers illustrates the advantages of this nonclassical IMD performance, as reported by Pengelly *et al.* [10]. The authors present, among several examples, a 900-MHz pHEMT amplifier with a saturated power of 41.5 dBm, operating from a

TABLE I

DEVICE	f_{OP} (MHz/GHz)	BIAS CONDITION (V/%I_{DSS})	$P_{1\mathrm{DB}}$ (dBm)	BACKOFF (dB)	EQUIVALENT IP3 (dBm)
LP1500	900 MHz	5/25%	23	−20	39
LP1500	1900	5/25%	22	−20 to +1	40–42
LP1500	50–2000	5/33%	25	−15	42
LP1500	8 GHz	8/33%	28	−12 to 0	38–45
LP6872	8–12	4/33%	20	−20	36–38
LP7612	18	5/33%	18	−10 to +1	28–34

supply voltage of 6.5 V. This amplifier, operated at 40 dBm, produced IMD products less than −35 dBc, which is equivalent to an IP3 of at least 57.5 dBm using (11b). Although the $P_{1\,\mathrm{dB}}$ was not specifically stated, it may be assumed to be in the range 39–41 dBm and, thus, the IP3 is at least 16.5 dB over the linear power $P_{1\,\mathrm{dB}}$, and possibly as much as 20 dB higher. The ACPR of this amplifier measured at −45 dBc, when operated at 38-dBm output power in the IS-95 CDMA forward-link mode (1.25-MHz offset). Clearly, the power backoff needed for the more stringent forward-link mode, approximately 2–3 dB, is significantly less than that required for other devices.

VIII. Limitations of the Extended Theory

While the extended theory does provide additional valuable insight, it does not yet provide a complete analytical model of the pHEMT over all modes of operation. There are two obvious enhancements that could be added to the theory; first, higher order terms could be added to the series expansion and, second, the AM-to-PM mechanism for the pHEMT could be modeled. It is expected that higher order terms (e.g., the k_7 term) become important in large-signal operation and, clearly, an analytical expression could be developed to account for these.

A more interesting issue is the understanding and modeling of the pHEMT's nonlinear reactive elements, such as the gate–source capacitance C_{GS}. In traditional FET large-signal models, such as the Curtice–Ettenberg formulation, the C_{GS} element is modeled as a simple junction capacitance, as described in [8, pp. 314–347]. This is not an adequate model for the pHEMT, again, because of its unique charge–control mechanism; nonlinear reactive elements such as this must be modeled and thereby incorporated into the theory. Further work is underway to explore and understand these unusual attributes of the pHEMT.

IX. Summary

An extension of the classical IMD theory has been developed that models the power transfer and IMD behavior of pHEMT devices, based on the specifics of the device's transconductance characteristics. Amplifiers utilizing pHEMT devices consistently achieve IMD performance that is 8–12 dB below classical expectations, over a wide dynamic range, even up to compression and saturation. Harmonic tuning may enhance this intrinsic performance beyond the results presented here. The extended theory provides for a reasonably good model of device behavior over a wide range of input power levels, but does not adequately predict the observed IMD performance under conditions of large-signal operation.

APPENDIX

The two-tone input signal from (6) may be expressed as

$$e_i = 2A\cos\left[\frac{1}{2}(\omega_1+\omega_2)t\right]\cos\left[\frac{1}{2}(\omega_1-\omega_2)t\right] \quad \text{(A1)}$$

with the following definitions:

$$\alpha \equiv \omega_1+\omega_2$$
$$\beta \equiv \omega_1-\omega_2.$$

Substitution of (A1) into (12) yields

$$\begin{aligned} e_o = {} & 2k_1A\cos\left(\frac{1}{2}\alpha t\right)\cos\left(\frac{1}{2}\beta t\right) \\ & + k_2A^2\left\{\left(\cos\left(\frac{1}{2}\alpha t\right)+1\right)\left(\cos\left(\frac{1}{2}\beta t\right)+1\right)\right\} \\ & + \frac{1}{2}k_3A^3\left\{\left[\cos\left(\frac{3}{2}\alpha t\right)+3\cos\left(\frac{1}{2}\alpha t\right)\right]\right. \\ & \qquad \left.\cdot\left[\cos\left(\frac{3}{2}\beta t\right)+3\cos\left(\frac{1}{2}\beta t\right)\right]\right\} \\ & + \frac{1}{4}k_4A^4\{\quad\} + \frac{1}{8}k_5A^5 \\ & \cdot\left\{\left[\cos\left(\frac{5}{2}\alpha t\right)+5\cos\left(\frac{3}{2}\alpha t\right)+10\cos\left(\frac{1}{2}\alpha t\right)\right]\right. \\ & \qquad \left.\cdot\left[\cos\left(\frac{5}{2}\beta t\right)+5\cos\left(\frac{3}{2}\beta t\right)+10\cos\left(\frac{1}{2}\beta t\right)\right]\right\}. \end{aligned} \quad \text{(A2)}$$

Using the trigonometry identity

$$2\cos(\theta)\cos(\phi) = \cos(\theta+\phi)+\cos(\theta-\phi).$$

From (A2), terms of the form $\cos((1/2)\alpha t)\cos((1/2)\beta t)$ yield terms containing ω_1 or ω_2, while terms of the form containing $\cos((3/2)\alpha t)\cos((1/2)\beta t)$ or $\cos((1/2)\alpha t)\cos((3/2)\beta t)$ product the third-order products of interest. All other combinations of terms (such as those is the k_4 expression) combine to give second-order products or higher harmonics. Collecting the terms of interest

$$\begin{aligned} e_0 \cong {} & \left\{k_1+\frac{9}{4}k_3A^3+\frac{25}{4}k_5A^5\right\}\cos(\omega_1 t) \\ & + \left\{k_1+\frac{9}{4}k_3A^3+\frac{25}{4}k_5A^5\right\}\cos(\omega_2 t) \\ & + \left\{\frac{3}{4}k_3A^3+\frac{25}{8}k_5A^5\right\}\cos\Big[(2\omega_1-\omega_2)t\Big] \\ & + \left\{\frac{3}{4}k_3A^3+\frac{25}{8}k_5A^5\right\}\cos\Big[(2\omega_2-\omega_1)t\Big]. \end{aligned} \quad \text{(A3)}$$

ACKNOWLEDGMENT

The author wishes to recognize the contributions and support of G. Vendelin, B. Ireton, E. Chan, T. LaRocca, M. Echeagaray, M. Yannuzzi, P. Mendoza, N. Mark, W. Vongchanh, T. Tran, and M. Bailey.

REFERENCES

[1] *Mobile station—Base station compatibility standard for dual-mode wideband spread spectrum cellular system*, TIA/EIA/IS-95 Interim Standard, July 1993.
[2] J. S. Kenny and A. Leke, "Power amplifier spectral regrowth for digital cellular and PCS applications," *Microwave J.*, pp. 74–92, Oct. 1995.
[3] T. T. Ha, *Solid-State Microwave Amplifier Design*, New York: Wiley, 1981, pp. 203–209.
[4] N. Blachman, "Bandpass nonlinearities," *IEEE Trans. Inform. Theory*, vol. IT-10, pp. 162–164, Apr. 1964.
[5] J. A. Higgins and R. L. Kuvas, "Analysis and improvement of intermodulation distortion in GaAs power FET's," *IEEE Trans. Microwave Theory Tech.*, vol. MTT-28, pp. 9–17, Jan. 1980.
[6] C. A. Liechti, "Microwave field-effect transistors—1976," *IEEE Trans. Microwave Theory Tech.*, vol. MTT-24, pp. 279–300, June 1976.
[7] G. Vendelin, *Design of Amplifiers and Oscillators by the S-Parameter Method*, New York: Wiley, 1982, pp. 10–14.
[8] S. M. Sze, *Physics of Semiconductor Devices*, New York: Wiley, 1981.
[9] M. J. Bailey, "Discrete pHEMT devices," Filtronic Solid State , Santa Clara, CA, Applicat. Notes, Aug. 1996.
[10] R. S. Pengelly, R. B. Binder, J. R. Griffiths, M. Virostko, and M. McPartlin, "pHEMT MMIC power amplifiers for base stations and adaptive arrays," *Appl. Microwave Wireless*, vol. 11, no. 1, pp. 30–41, Jan. 1999.

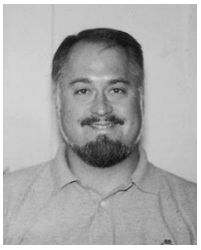

Michael Jon Bailey (M'94) was born in San Diego, CA, in 1957. He received the B.A. degree in physics from the University of California at San Diego, in 1979, the M.A. degree in physics from the University of California at Santa Barbara, in 1981, the Degree of Engineer in electrical engineering from Stanford University, Stanford, CA, in 1992, and is currently working toward the M.B.A. degree at Santa Clara University, Santa Clara, CA.

In 1982, he joined Teledyne Microwave, Mountain View, CA, as an Applications Engineer, where he first became involved with pHEMT device technology. In 1987, he joined Varian Solid State, Santa Clara, CA, where he was initially involved with GaAs IMPATT diodes. His work resulted in the development of a new heterojunction IMPATT diode structure, and holds two U.S. patents in this area. In 1994 he returned to an involvement with three-terminal devices, and is currently the Product Engineer Manager of the Handset Products Engineering Group, Filtronic Solid State, Santa Clara, CA. His current interest include the modeling of the nonlinear mechanisms of InGaAs/AlGaAs pHEMT devices, and the implications for new-generation communications systems.